PCCP

Accepted Manuscript

ROYAL SOCIETY OF CHEMISTRY

www.rsc.org/pccp

Temperature-Dependent Dynamics of Water in Aqueous $NaPF_6$ Solution

Dayoung Nam,[1] Chiho Lee,[1] and Sungnam Park[1,2*]

[1]Department of Chemistry, Korea University, Seoul 136-713, Korea.

[2]Multidimensional Spectroscopy Laboratory, Korea Basic Science Institute, Seoul 136-713, Korea.

[*]Authors to whom correspondence should be addressed.
Email addresses: spark8@korea.ac.kr

Abstract

Dynamics of water in bulk and ionic hydration shells in aqueous ionic solutions are different due to the local environments as can be expected. However, direct measurements of the dynamics of water in ionic hydration shells apart from those of bulk water have been experimentally quite challenging because of the poor spectral distinction among water molecules in bulk and ionic hydration shells. Very interestingly, the hydroxyl stretch band in the FTIR spectrum of aqueous $NaPF_6$ solution was able to be resolved into the contributions from three distinct subsets of water: (1) water molecules hydrogen-bonded to other water (i.e., bulk water), (2) water molecules in the hydration shells Na^+ ions (i.e., cationic hydration shell), and water molecules hydrogen-bonded to PF_6^- ions (i.e., anionic hydration shell). Therefore, such spectral features enabled us to study the individual dynamics of water in different subsets in aqueous $NaPF_6$ solution. IR pump-probe spectroscopy was used to measure vibrational population relaxation, $P(t)$, and orientational anisotropy decay, $r(t)$, of water in different subsets. The vibrational lifetimes of water in cationic and anionic hydration shells in aqueous 5.0 M $NaPF_6$ solution were directly determined and found to be independent of temperature up to 50 °C. Orientational anisotropy decay of water in ionic hydration shells were observed to be much slower than in bulk. $r(t)$ became faster with increasing temperature as predicted by the Debye-Stokes-Einstein equation. The activation energies for water orientation in different subsets were measured and found to be not much different in cationic and anionic hydration shells. In our current experiments, the dynamics of water in bulk and ionic hydration shells in aqueous $NaPF_6$ solutions were able to be studied in more detail.

I. Introduction

Hydrogen-bond (H-bond) structure and dynamics of water are sensitively dependent on the local environments of the probing water molecules and thus can provide the information on their local environments, such as charged or polar interfaces as well as hydrophobic or hydrophilic environments.[1-4] In aqueous ionic solutions, water molecules form hydration shells around dissolved ions and water molecules in cationic and anionic hydration shells may have dynamic properties different from those in bulk. To understand the effect of ions on the structure and dynamics of water, a variety of aqueous ionic solutions have been extensively studied.[5-13] To study the H-bond structure and dynamics of water, the hydroxyl stretch band (–OH or –OD) of isotopically diluted water (HOD in H_2O or D_2O) has been used as a vibrational probe.[10, 14-17] The hydroxyl stretch band of aqueous ionic solutions appears simply as a broad peak reflecting that water molecules in bulk and ionic hydration shells are not spectrally well resolved. This is because the hydroxyl stretch peaks of water in bulk and hydration shells are very broad and significantly overlapped.[7] Accordingly, there has been an experimental difficulty in separately measuring the dynamics of water in bulk and ionic hydration shells in aqueous ionic solutions. What has been measured with most of aqueous ionic solutions by probing the hydroxyl stretch peak is weighted-averaged dynamics of water in bulk and ionic hydration shells. If the dynamics of water in cationic and anionic hydration shells were separately measured, it would give more detailed information on the properties of aqueous ionic solutions, the dynamics of water at the charged surfaces of proteins, and Hofmeister ionic effects.[18-20] In aqueous ionic solutions with BF_4^-, ClO_4^-, and PF_6^- ions, the hydroxyl stretch band was found to be split into two peaks and H-bond exchange dynamics were studied.[17, 21-24] Recently, we have studied the H-bond exchange dynamics in aqueous $NaPF_6$ solution by two-dimensional infrared (2DIR) spectroscopy.[24] Interestingly, water molecules in aqueous $NaPF_6$ solution are spectrally separated into two subsets of water that

are H-bonded to either other water molecules or PF_6^- ions. This spectral feature gave an opportunity to investigate the individual subsets of water as well as inter-conversion dynamics between them.[24]

In this work, we further studied the H-bond structure and dynamics of water in aqueous $NaPF_6$ solution by using FTIR and IR pump-probe (IR PP) experiments. $NaPF_6$ salt was dissolved in 8% HOD in H_2O and the OD stretch band of HOD was probed. In the FTIR spectrum of aqueous 5.0 M $NaPF_6$ solution in Figure 1, the OD stretch band is split into a broad peak at ~2530 cm^{-1} and a narrow peak at ~2670 cm^{-1}. The narrow peak at ~2670 cm^{-1} comes from the water molecules in the hydration shells of PF_6^- ions (OD_A). On the other hand, the broad peak at ~2530 cm^{-1} is associated with water molecules in bulk and the hydration shells of Na^+ ions.[24] Therefore, as shown in Figure 1(B), the broad peak at ~2530 cm^{-1} can be further decomposed into two subsets of water based on the two-state model: (1) HOD molecules in bulk (OD_W) and (2) HOD molecules in the hydration shell of Na^+ ions (OD_C). The OD stretch band of HOD in aqueous 5.0 M $NaPF_6$ solution was able to be spectrally separated into the contributions from three subsets of water (OD_W, OD_C, and OD_A). Here, we performed FTIR and IR pump-probe (IR PP) experiments with aqueous 5.0 M $NaPF_6$ solution at different temperatures and measured the effect of temperature on the dynamics of water in different subsets in aqueous 5.0 M $NaPF_6$ solution. In our present experiments, the individual dynamics of water in ionic hydration shells and bulk were able to be studied in greater detail.

II. Experimental methods

A. Sample preparation

$NaPF_6$ (98% purity) and D_2O (99.9% purity) were purchased from Sigma Aldrich and used as received. Isotopically diluted water was prepared by mixing D_2O and H_2O with 4:96 volume

ratio producing 8% HOD in H_2O. Aqueous 5.0 M $NaPF_6$ solution was prepared by directly dissolving $NaPF_6$ salt in 8% HOD in H_2O. For the background correction, a reference solution with the same molar concentration of $NaPF_6$ salt dissolved in neat H_2O was prepared. For IR experiments, the home-made IR cell with two 3 mm thick CaF_2 windows and a 25 μm Teflon spacer.

B. Fourier transform infrared (FTIR) spectroscopy

FTIR spectra of the sample solutions were measured by using a Varian 640-IR spectrometer in the range of 400-4000 cm^{-1} with a resolution of 1 cm^{-1}. Temperature-dependent FTIR experiments were carried out with 0.0 M and 5.0 M $NaPF_6$ solutions by varying the temperature from 25 to 50 °C with an interval of 5 °C. The temperature of the sample solutions was able to be varied by 0.1 °C by our temperature controller. In order to ensure thermal equilibrium of the sample cell, the temperature of the sample cell was kept at least for 15 minutes for a given temperature before the FTIR spectrum was taken. After the temperature-dependent FTIR experiments, the sample cell was quickly cooled to room temperature by using a fan and the FTIR spectrum was measured again. We compared two FTIR spectra of the sample measured before and after temperature-dependent FTIR experiments to check any undesired degradation of the sample solution during the experiments.

C. IR pump-probe spectroscopy

Our femtosecond mid-IR laser system was presented in detail elsewhere.[25, 26] Briefly, 800 nm pulses with ~45 fs duration and ~1.0 mJ per pulse were generated by a Ti:sapphire oscillator (Tsunami, Spectra-Physics) and regenerative amplifier (Spitfire, Spectra-Physics) laser

system operating at 1 kHz. The 800 nm pulses were down-converted by optical parametric amplifier (OPA, Spectra-Physics) to near-IR pulses at ~1.4 and ~1.9 μm which were mixed in a 0.5 mm thick $AgGaS_2$ crystal (Type II) producing mid-IR pulses by difference frequency generation. The power spectrum of the mid-IR pulses had a Gaussian envelope with a ~ 250 cm^{-1} bandwidth (full width at half maximum, FWHM). The center frequency of the mid-IR pulses was tuned by changing the orientation of the BBO (β-barium borate) and $AgGaS_2$ crystals relative to the incident pulses in the OPA. The CaF_2 plates with different thicknesses were used to compensate for the linear dispersion introduced by other dielectric materials in the experimental setup including a Ge Brewster plate and ZnSe beam splitters. The mid-IR pulses were transform-limited at the sample.

A He-Ne laser was used to align all optics in the setup. The mid-IR pulses were overlapped with a mode-matched He-Ne alignment beam by using the Ge plate. A ZnSe beam splitter with a 9:1 intensity ratio was used to split the mid-IR beam into pump and probe beams. Before the sample, the pump and probe beam pathways had the wire grid polarizers (P_1 and P_2) where the polarization states were set to be 0° and 45° of the normal to the optical table, respectively. These beams were focused onto the sample by a concave mirror (focal length, f.l. = 100 mm). The probe beam passed through the analyzer wire grid polarizer (P_3) on a motorized rotational state after the sample and its polarization states (0° and 90°) were set to measure the parallel and perpendicular IR pump-probe (IR PP) signals by using computer-controlled motorized rotational stage. This beam was collimated by a concave mirror (f.l. = 100 mm) and dispersed through a monochromator onto the 64-element mercury-cadmium-telluride (MCT) array detector. The polarization of the probe beam was parallel and perpendicular to that of the pump beam was used to measure the parallel and perpendicular IR PP signals, $S_{\parallel}(\omega_{pr},t)$ and $S_{\perp}(\omega_{pr},t)$, respectively.

III. Results and discussion

A. FTIR study

Figure 1(A) displays the OD stretch band in the FTIR spectra measured with 0.0 and 5.0 M $NaPF_6$ solutions. When compared with 8% HOD in H_2O (0.0 M), the OD band is split into two peaks in aqueous 5.0 M $NaPF_6$ solution. In addition, the low frequency peak is blue-shifted and the high frequency peak newly appears. In aqueous 5.0 M $NaPF_6$ solution, the narrow peak at ~2670 cm^{-1} comes from the HOD molecules in the hydration shell of PF_6^- ions while the broad peak comes from water molecules in bulk and the hydration shells of Na^+ ions. Accordingly, the OD stretch band in the FTIR spectrum, $S(\omega)$, is decomposed into three contributions,

$$S(\omega) = \alpha \cdot S_{OD_W}(\omega) + A_1 \cdot S_{OD_C}(\omega) + A_2 \cdot S_{OD_A}(\omega) \quad (1)$$

where α is the scaling factor, $S_{OD_W}(\omega)$ is the FTIR spectrum measured at 0.0 M, $S_{OD_C}(\omega)$ and $S_{OD_A}(\omega)$ are the pseudo-Voigt profiles to fit the OD_C and OD_A, respectively (See the Supporting Information for detail). Among these three contributions (OD_W, OD_C, and OD_A), the OD_A peak is positioned separately at ~2670 cm^{-1} while the broad peak at ~2530 cm^{-1} consists of the OD_W and OD_C. Therefore, the decomposition of the low frequency peak at ~2530 cm^{-1} into the OD_W and OD_C contributions is a key analysis. In aqueous halide solutions, the OD_W, OD_C, and OD_A contributions are significantly overlapped and it is practically impossible to spectrally separate them. However, in aqueous 5.0 M $NaPF_6$ solution, the decomposition of the OD band into three contributions is readily possible as shown in Figure 1(B). Three OD peaks shown in Figure 1(B) can be thought of as the eigen spectra of the OD_W, OD_C, and OD_A contributions. The water molecules in cationic hydration shells (OD_C) appear at the higher frequency relative to the bulk water (OD_W). The blue shift

of the low frequency peak in Figure 1(A) results from the fact that the water molecules in bulk participate in the hydration of Na^+ ions.

Figures 2(A) and 2(B) show the FTIR spectra of 0.0 and 5.0 M $NaPF_6$ solutions measured at different temperatures, respectively. In Figure 2(A), the OD_W peak gradually blue shifts and its amplitude decreases as the temperature is raised. The blue shift of the OD_W peak results from the weakening of H-bond structures due to the thermal energy with increasing temperature. The amplitude of the OD_W peak decreases due to the non-Condon effect.[27, 28] In Figure 2(B), the low frequency peak (OD_W + OD_C) show the behavior very similar to the OD_W peak shown in Figure 2(A) whereas in the case of the OD_A peak its amplitude is slightly decreased without a significant change in its peak position. For further detailed analysis, the FTIR spectrum at a given temperature was decomposed into three contributions by using Eq. (1) and the spectral decomposition analyses are summarized in Table 1 and presented in Figure S1 (in the Supporting Information). As shown in Table 1, the positions of the OD_C, and OD_A peaks in aqueous 5.0 M $NaPF_6$ solution are almost the same while the position of the OD_W peak gradually blue shifts as indicated in Figure 2(A). In Figure 3, the areas and widths of the OD_W, OD_C, and OD_A peaks are plotted as a function of temperature. As the temperature is increased, the spectral features of the OD_W peak are more dramatically changed when compared with the OD_C, and OD_A peaks. These results imply that the H-bond structures of water in cationic and anionic hydration shells are more rigid and less influenced by the temperature than that of bulk water.

B. IR pump-probe study

In IR pump-probe (IR PP) experiments, the molecules on the ground state (υ=0) are excited to the first excited state (υ=1) by a strong pump pulse and the relaxation of the excited molecules is monitored by the time-delayed probe pulse. IR PP signals decay due to

vibrational population relaxation and orientational relaxation. Vibrational population relaxation dynamics, $P(t)$, and orientational relaxation dynamics, $r(t)$, are separately measured by polarization-controlled IR PP experiments in which IR PP signals are collected in parallel and perpendicular beam polarization geometries.[29] The IR PP signals measured with aqueous 5.0 M $NaPF_6$ solution were found to decay to a constant offset due to the heating effect, which was readily taken into account in the analysis of IR PP signals.[30-33] By including the heating contribution, the parallel and perpendicular IR PP signals, $S_{\parallel}(t)$ and $S_{\perp}(t)$, are written at a given probe frequency, respectively, by

$$S_{\parallel}(t) = P(t)\left(1+\frac{4}{5}C_2(t)\right)+G(t) \tag{2}$$

$$S_{\perp}(t) = P(t)\left(1-\frac{2}{5}C_2(t)\right)+G(t) \tag{3}$$

where $P(t)$ is the vibrational population relaxation, $C_2(t)$ is the orientational correlation function and is represented by the second-order Legendre polynomial of the transition dipole correlation function, $C_2(t)=\left\langle P_2\left[\mu(t)\cdot\mu(0)\right]\right\rangle$, and $G(t)$ represents the heating contribution which appears as a constant offset at long times. The isotropic IR PP signal, $S_{\mathrm{iso}}(t)$, is given by

$$S_{\mathrm{iso}}(t)=\frac{S_{\parallel}(t)+2S_{\perp}(t)}{3}=P(t)+G(t) \tag{4}$$

Figure 4 shows the frequency-resolved isotropic IR PP signal, $S_{\mathrm{iso}}(\omega_{\mathrm{pr}},t)$, measured with 5.0 M $NaPF_6$ solution at 40 ºC. To extract the vibrational population relaxation and orientational relaxation dynamics, IR PP signals are analyzed at the maxima of the low and high frequency peaks. To obtain the vibrational population relaxation, $P(t)$, the heating contribution, $G(t)$,

needs to be subtracted from the isotropic IR PP signal, $S_{\mathrm{iso}}(t)$, as shown in Figures 4(B) and 4(C). And the heating contribution, $G(t)$, in Eq. (4) is modeled by[32]

$$G(t)=\frac{\alpha}{k_{\mathrm{r}}-k_{\mathrm{b}}}\left[k_{\mathrm{r}}\left(1-\exp(-k_{\mathrm{b}}t)\right)+k_{\mathrm{b}}\left(-1+\exp(-k_{\mathrm{r}}t)\right)\right] \quad (5)$$

where $k_{\mathrm{r}}=1/T_1$ and k_{b} is the rate constant for relaxation of an intermediate state to a hot ground state leading to a constant offset at long times, α. Finally, vibrational population decay, $P(t)$, and orientational anisotropy decay, $r(t)$, can be obtained by[32]

$$P(t)=\frac{S_{\parallel}(t)+2S_{\perp}(t)}{3}-G(t) \quad (6)$$

$$r(t)=\frac{S_{\parallel}(t)-S_{\perp}(t)}{S_{\parallel}(t)+2S_{\perp}(t)-3G(t)} \quad (7)$$

In our IR PP experiments, the vibrational population decay of the OD stretch mode of HOD in neat water was well fit by a single exponential function with a vibrational lifetime of T_1=1.7 ± 0.1 ps while the orientational anisotropy decay of HOD molecule in neat water was also well fit by a single exponential function with an orientational relaxation time constant of τ_{or}=2.5 ± 0.2 ps. These values agree well with the values reported previously.[7, 8, 33]

B-1. Population relaxation dynamics

Figures 5(A) and 6(A) show the population relaxation dynamics measured with aqueous 5.0 M $NaPF_6$ solution at different temperatures. An interesting observation is that $P(t)$ measured at the low frequency (~2530 cm^{-1}) and high frequency (~2670 cm^{-1}) are almost identical within our experimental error as the temperature is raised up to 50 °C as shown in Figures 5(A) and 6(A). This implies that the vibrational lifetimes are independent of temperature. $P(t)$ of the low and high frequency peaks were readily represented by the first-order kinetics, $P(t)=A\cdot\exp(-t/T_1)$. The vibrational lifetime of the low frequency peak was determined to

be $T_1 = 2.4$ ps while the vibrational lifetime of the high frequency peak was determined to be $T_1 = 6.6$ ps .

As discussed earlier and shown in Figure 1(B), the low frequency peak is composed of OD_W and OD_C. Therefore, $P(t)$ of the low frequency peak was further analyzed by using the two-state model,

$$P(t) = a_1 \cdot \exp\left(-\frac{t}{T_{1,OD_W}}\right) + a_2 \cdot \exp\left(-\frac{t}{T_{1,OD_C}}\right) \quad (8)$$

where the first and second terms describe the population decay of OD_W and OD_C, respectively, with $a_1 + a_2 = 1$. In this analysis, the population decay of the low frequency peak is assumed to be represented as the sum of the population decays of the OD_W and OD_C with relative concentration ratios. The vibrational lifetime of OD_W was fixed by $T_{1,OD_W} = 1.7$ ps, which was measured from neat water (0.0 M). By fitting $P(t)$ of the low frequency peak by Eq. (8), the vibrational lifetimes of OD_W and OD_C were determined to be $T_{1,OD_W} = 1.7$ ps (a_1=0.62) and $T_{1,OD_W} = 3.7$ ps (a_2=0.38), respectively. In short, three subsets of water (OD_W, OD_C, and OD_A) in aqueous 5.0 M $NaPF_6$ solution are found to be spectrally distinct and have their unique lifetimes ($T_{1,OD_W} = 1.7$ ps, $T_{1,OD_C} = 3.7$ ps, and $T_{1,OD_A} = 6.6$ ps), which are independent of temperature.

B-2. Orientational relaxation dynamics

As shown in Figures 5(B), and 6(B), orientational relaxation dynamics of the low and high frequency peaks are found to be significantly dependent on the temperature of aqueous $NaPF_6$ solution. The orientational anisotropy decay, $r(t)$, of water gets faster as the temperature rises because the orientational motion of water is facilitated by the thermal energy and the H-bonds get weaker at higher temperatures. Orientational relaxation dynamics

of water in aqueous solutions are known to play critical roles in the global rearrangements of the H-bond network which are accomplished by transiently breaking and reforming the H-bonds on picosecond time scales. $r(t)$ of water in bulk is well known to be described by a single exponential function with τ_{or}= 2.6 ps. In contrast, $r(t)$ of water in aqueous ionic solutions is normally well represented by a bi-exponential function. In the literatures, the bi-exponential behaviors of $r(t)$ of water in aqueous ionic solutions are often described as two sequential orientational diffusion processes in the wobbling-in-a-cone model.[2] Accordingly, the orientational anisotropy decays measured in our current experiments were fitted by the bi-exponential function,

$$r(t) = b_1 \exp(-t/\tau_{or1}) + b_2 \exp(-t/\tau_{or2}) \quad (9)$$

where $\tau_{or1} < \tau_{or2}$. The results of bi-exponential fit to $r(t)$ are summarized in Tables 2 and 3. At 22 ^{o}C, the orientational relaxation of the high frequency peak (OD_A, τ_{or2}=7.6 ps) is slower than that of the low frequency peak (OD_W+OD_C, τ_{or2}=6.6 ps). The long time component (τ_{or2}) of $r(t)$ is associated with the overall orientational relaxation, which is known to be well described by the Debye-Stokes-Einstein (DSE) equation.[26] By comparing the long time components of $r(t)$, the orientational relaxation of water in ionic hydration shells are found to be much slower although it is not straightforward to extract the orientational relaxation time constant of each subset from our experimental results.

To determine the activation energies of the overall orientational relaxation (τ_{or2}), an Arrhenius plot can be used in the following form,[34-37]

$$\ln\left(\frac{1}{\tau_{or}}\right) = \ln\left(\frac{1}{\tau_{or,0}}\right) - \frac{E_a}{R}\frac{1}{T} \quad (10)$$

where E_a is the activation energy for the overall orientational relaxation and τ_{or} is the orientational relaxation time, which is related to the orientational rate constant (k_{or}=1/τ_{or}). In

Eq. (10), $\tau_{or,0}$ is the orientational relaxation time in the absence of any activation energy. The Arrhenius plots for τ_{or2} are shown in Figure 7. The activation energies for the overall orientational relaxation are determined to be 15.7 kJ/mol for the low frequency peak and 16.6 kJ/mol for the high frequency peak, respectively. Our experimental values are in the range of the activation energies that were previously determined with other aqueous solutions.[35-38]

The activation energy for water orientation should be related to the strengths of H-bonds or intermolecular interactions (between cation and water), which might be expected to be quite different in cationic hydration shells (or bulk) and in anionic hydration shells. The H-bond energy between water molecules is ~ 21 kJ/mol.[39, 40] The H-bond between water and PF_6^- ion is weaker than the H-bond between water molecules. Bakker and coworkers reported that the activation energy for water orientation in bulk was measured to be 17±2 kJ/mol.[35] Therefore, our current results combined with their results indicate that the activation energies of water orientation in bulk (OD_W), cationic hydration shell (OD_C), and anionic hydration shell (OD_A) are not much different. This is an interesting results because the orientational relaxation times of water in three subsets are all different but their activation energies are similar. In aqueous solutions, orientational relaxation of water occurs by continuously breaking and reforming H-bonds. Recent molecular dynamics simulation results indicate that H-bond exchange processes in aqueous solutions occur by orientational jump mechanism of water molecules in which the availability of new incoming H-bond acceptors and the energy difference between two H-bond configurations before and after H-bond exchange are important as well.[41-43] Therefore, the activation energy for water orientation is not necessarily correlated only with the H-bond energy or water-ion interactions but it should be understood by including all the mechanistic processes through which the orientation relaxation takes place.

Before this section is closed, it is worthwhile to mention that in contrast to the vibrational population relaxation, the orientational relaxation of water in aqueous $NaPF_6$ solution may not be well described by the sum of three contributions (OD_W, OD_C, and OD_A). As mentioned above, the orientational relaxation involves the inter-conversions among three subsets of water by breaking and reforming H-bonds in a complicated manner and thus three contributions are intermingled when it comes to the orientational relaxation. In addition, the orientational relaxation time is sensitively dependent on both the viscosity (η) and temperature (T) of the solution based on the Debye-Stokes-Einstein (DSE) equation,[26]

$$\tau_{or} = \frac{\eta V f C_f}{k_B T} \qquad (11)$$

where k_B and T are the Boltzmann constant and the temperature, respectively, and V is the van der Waals volume of a solute. f is the shape factor introduced by Perrin[44] to relate to the ratio of the major and minor axes of the nonspherical shape of the solute.[45] C_f is the friction coefficient that determines the extent of coupling between the solute and the neighboring solvents.[46] Based on the DSE equation, τ_{or} is proportional to η/T. To fully understand the temperature dependence of τ_{or}, $\eta(T)$ needs to be determined as well.

IV. Summary and Concluding Remarks

Both cations and anions have substantial influences on the H-bond structures and dynamics of water in aqueous ionic solutions. However, the individual effects of cations and anions on the H-bond structures and dynamics of water are not necessarily the same and need to be separately measured for better understanding the overall properties of aqueous ionic solutions and the behaviors of water molecules at charged interfaces such as protein surfaces, lipid bilayers, and reverse micelles. In this work, H-bond structures and dynamics of water in aqueous 5.0 M $NaPF_6$ solution were investigated by using FTIR and IR pump-probe

experiments. Temperature-dependent FTIR experiments were performed for quantitative spectral analyses of different subsets of water in aqueous $NaPF_6$ solutions. Polarization-controlled IR PP spectroscopy was used to study the vibrational population relaxation and orientational relaxation dynamics of water in three different subsets (OD_W, OD_C, and OD_A) in aqueous $NaPF_6$ solutions. The vibrational lifetimes of OD_W, OD_C, and OD_A were directly determined and found to be independent of temperature up to 50 °C. However, the orientational relaxation dynamics of OD_W, OD_C, and OD_A were a little more complicated to be simply described as for the vibrational population relaxation. In general, $r(t)$ of OD_C and OD_A were much slower than that of OD_W, and $r(t)$ of OD_W, OD_C, and OD_A got faster with increasing temperature. By using the Arrhenius-type plots, the activation energies for water orientation were determined and were not much different for OD_W, OD_C, and OD_A.

The results from FTIR study and population relaxation measurements indicate that three subsets of water show well-defined behaviors in terms of their spectral feature and unique vibrational lifetimes. In this case, FTIR spectrum and vibrational lifetime for a given subset of water are considered as static parameters depending on the identity of the subsets. On the other hand, the results of orientational anisotropy measurements imply that the overall orientational relaxation times of water in ionic hydration shells are longer than in bulk and the activation energies are not much different for three subsets. As opposed to the vibrational lifetimes, the orientational relaxation times, which are considered as dynamic parameters, are not well distinct or unique for different subsets and are also heavily dependent on the viscosity and temperature. The orientational relaxation is less structurally localized because it is accompanied by switching H-bond partners among different subsets leading to a global rearrangement of H-bond structure in aqueous ionic solutions.

Aqueous PF_6^- solution are a good model system to study the effects of ions on the dynamics of water because three subsets of water (i.e. OD_W, OD_C, and OD_A) can be

distinguished as presented in this work. Especially, the effects of cations on water dynamics, which have not been able to be separately investigated with other aqueous ionic solutions, can be better studied by using aqueous PF_6^- solutions with different cations such as Li^+, K^+, Mg^{2+}, NH_4^+, and so on.

Acknowledgements

This work was supported by the National Research Foundation of Korea (NRF) grants funded by the Korea government (MEST) (Nos. 2013R1A1A2009991 and 20100020209) and the KETEP grant (No. 20104010100640).

References

1. S. K. Pal and A. H. Zewail, *Chem. Rev.*, 2004, 104, 2099-2123.
2. H.-S. Tan, I. R. Piletic and M. D. Fayer, *J. Chem. Phys.*, 2005, 122, 174501(174509).
3. Y. Zhang and P. S. Cremer, *Curr. Opin, Chem. Biol.*, 2006, 10 658-663.
4. I. A. Heisler and S. R. Meech, *Science*, 2010, 327, 857-860.
5. A. W. Omta, M. F. Kropman, S. Woutersen and H. J. Bakker, *Science*, 2003, 301, 347-349.
6. M. F. Kropman and H. J. Bakker, *J. Am. Chem. Soc.*, 2004, 126, 9135-9141.
7. S. Park and M. D. Fayer, *Proc. Natl. Acad. Sci. USA*, 2007, 104, 16731-16738.
8. S. Park, D. E. Moilanen and M. D. Fayer, *J. Phys. Chem. B*, 2008, 102, 5279-5290.
9. Y. Marcus, *Chem. Rev.*, 2009, 109, 1346-1370.
10. K. J. Tielrooij, N. Garcia-Araez, M. Bonn and H. J. Bakker, *Science*, 2010, 328, 1006-1009.
11. K. J. Gaffney, M. Ji, M. Odelius, S. Park and Z. Sun, *Chem. Phys. Lett.*, 2011, 504, 1-6.
12. H. T. Bian, X. W. Wen, J. B. Li, H. L. Chen, S. Z. Han, X. Q. Sun, J. A. Song, W. Zhuang and J. R. Zheng, *Proc. Nat. Acad. Sci. USA*, 2011, 108, 4737-4742.
13. H. Kim, S. Park and M. Cho, *Phys. Chem. Chem. Phys.*, 2012, 14, 6233-6240.
14. S. Woutersen and H. J. Bakker, *Nature*, 1999, 402, 507-509.
15. C. J. Fecko, J. D. Eaves, J. J. Loparo, A. Tokmakoff and P. L. Geissler, *Science*, 2003, 301, 1698-1702.
16. J. B. Asbury, T. Steinel, K. Kwak, S. A. Corcelli, C. P. Lawrence, J. L. Skinner and M. D. Fayer, *J. Chem. Phys.*, 2004, 121, 12431-12446.
17. M. Ji, M. Odelius and K. J. Gaffney, *Science*, 2010, 328, 1003.
18. R. Perez-Jimenez, R. Godoy-Ruiz, B. Ibarra-Molero and J. M. Sanchez-Ruiz, *Biophys. J.* , 2004, 86, 2414-2429.

19. Y. Zhang, S. Furyk, D. E. Bergbreiter and P. S. Cremer, *J. Am. Chem. Soc.*, 2005, 127, 14505-14510.

20. P. Lo Nostro and B. W. Ninham, *Chem. Rev.*, 2012, 112, 2286-2322.

21. S. Park, M. Odelius and K. J. Gaffney, *J. Phys. Chem. B.*, 2009, 113, 7825-7835

22. D. E. Moilanen, D. Wong, D. E. Rosenfeld, E. E. Fenn and M. D. Fayer, *Proc. Natl. Acad. Sci.*, 2009, 106, 375–380.

23. M. Ji and K. J. Gaffney, *J. Chem. Phys.*, 2011, 134, 044516.

24. H. Son, D. Nam and S. Park, *J. Phys. Chem. B*, 2013, 117, 13604-13613.

25. H. Son, J. Haneul, S. R. Choi, H. W. Jung and S. Park, *J. Phys. Chem. B*, 2012, 116, 9152-9159.

26. H. Son, Y. Kwon, J. Kim and S. Park, *J. Phys. Chem. B* 2013, 117, 2748−2756.

27. J. R. Schmidt, S. A. Corcelli and J. L. Skinner, *J. Chem. Phys.*, 2005, 123, 044513(044513).

28. J. J. Loparo, S. T. Roberts, R. A. Nicodemus and A. Tokmakoff, *Chem. Phys.*, 2007, 341, 218-229.

29. K.-K. Lee, K.-H. Park, D. Kwon, J.-H. Choi, H. Son, S. Park and M. Cho, *J. Chem. Phys.*, 2011, 134, 064506.

30. E. T. J. Nibbering and T. Elsaesser, *Chem. Rev.*, 2004, 104, 1887−1914.

31. T. Steinel, J. B. Asbury, J. Zheng and M. D. Fayer, *J. Phys. Chem. A*, 2004, 108.

32. I. Piletic, D. E. Moilanen, D. B. Spry, N. E. Levinger and M. D. Fayer, *J. Phys. Chem. A*, 2006, 110, 4985-4999.

33. Y. L. A. Rezus and H. J. Bakker, *J. Chem. Phys.*, 2006, 125.

34. H.-K. Nienhuys, R. A. van Santen and H. J. Bakker, *J. Chem. Phys.*, 2000, 112, 8487-8494.

35. C. Petersen, K. J. Tielrooij and H. J. Bakker, *J. Chem. Phys.*, 2009, 130, 214511-214511.

36. R. A. Nicodemus, S. A. Corcelli, J. L. Skinner and A. Tokmakoff, *J. Phys. Chem. B*, 2011, 115, 5604-5616.

37. S. T. van der Post and H. J. Bakker, *J. Phys. Chem. B*, 2014, DOI: 10.1021/jp501240e, in press.

38. K. J. Tielrooij, C. Petersen, Y. L. A. Rezus and H. J. Bakker, *Chem. Phys. Lett.*, 2009, 471, 71-74.

39. D. Eisenberg and W. Kauzmann, *The Structure and Properties of Water*, Clarendon Press, Oxford, 1969.

40. S. Suresh and V. Naik, *J. Chem. Phys.*, 2000, 113, 9727-9732.

41. D. Laage and J. T. Hynes, *Science*, 2006, 311, 832-835.

42. D. Laage and J. T. Hynes, *Proc. Nat. Acad. Sci.*, 2007, 104, 11167-11172.

43. D. Laage, G. Stirnemann, F. Sterpone, R. Rey and J. T. Hynes, *Annu. Rev. Phys. Chem.*, 2011, 62, 395-416.

44. F. Perrin, *J. Phys. Radium*, 1934, 5, 497-511.

45. A. L. Sturlaugson, K. S. Fruchey, S. R. Lynch, S. R. Arago and M. D. Fayer, *J. Phys. Chem. B*, 2010, 114, 5350-5358.

46. C.-M. Hu and R. Zwanzig, *J. Chem. Phys.*, 1974, 60, 4354-4357.

Table 1. Analyses of FTIR spectra of aqueous 5.0 M $NaPF_6$ solution at different temperatures.

Temperature (ºC)		25 ºC	30 ºC	35 ºC	40 ºC	45 ºC	50 ºC
OD_W	Center (cm^{-1})	2507	2509	2511	2513	2515	2517
	Area	22.41	21.77	20.27	19.46	18.51	17.28
	Width (cm^{-1})	165.1	166.3	167.1	168.5	169.9	170.6
OD_C	Center (cm^{-1})	2545	2545	2545	2545	2545	2545
	Area	22.18	21.99	21.89	21.79	21.69	21.59
	Width (cm^{-1})	142.5	142.6	142.7	142.8	142.9	143.0
OD_A	Center (cm^{-1})	2669	2669	2669	2669	2669	2669
	Area	7.32	7.18	7.09	7.00	6.92	6.83
	Width (cm^{-1})	29.88	29.91	30.00	30.10	30.20	30.30

Table 2. Analyses of vibrational population decays, $P(t)$, and orientational anisotropy decays, $r(t)$, of the low frequency peak (OD_W + OD_C) at different temperatures.

	ω_{pr} (cm^{-1})	T_1 (ps)	b_1	τ_{or1} (ps)	b_2	τ_{or2} (ps)
22 ºC	2520	2.4±0.2	0.10±0.02	0.65±0.1	0.28±0.03	6.6±0.4
30 ºC	2523	2.3±0.2	0.08±0.02	0.53±0.1	0.28±0.03	5.4±0.4
40 ºC	2529	2.3±0.2	0.10±0.02	0.43±0.1	0.27±0.03	4.5±0.4
50 ºC	2535	2.3±0.2	0.12±0.02	0.34±0.1	0.26±0.03	3.7±0.4

Table 3. Analyses of vibrational population decays, $P(t)$, and orientational anisotropy decays, $r(t)$, of the high frequency peak (OD_A) at different temperatures.

	ω_{pr} (cm^{-1})	T_1 (ps)	b_1	τ_{or1} (ps)	b_2	τ_{or2} (ps)
22 ºC	2670	6.6±0.2	0.10±0.01	0.35±0.1	0.21±0.01	7.6±0.2
30 ºC	2670	6.6±0.2	0.19±0.01	0.36±0.1	0.17±0.01	6.3±0.2
40 ºC	2670	6.6±0.2	0.19±0.01	0.35±0.1	0.15±0.01	5.3±0.2
50 ºC	2670	6.5±0.2	0.22±0.01	0.46±0.1	0.12±0.01	4.2±0.2

Figure captions

Figure 1. (A) The OD stretch band in FTIR spectra measured with neat water and aqueous 5.0 M $NaPF_6$ solution. (B) Decomposition of FTIR spectrum of 5.0 M $NaPF_6$ solution into three contributions.

Figure 2. FTIR spectra measured with (A) neat water and (B) aqueous 5.0 M $NaPF_6$ solution with increasing the temperature from 25 ºC to 50 ºC with an interval of 5 ºC.

Figure 3. Decomposition of temperature-dependent FTIR spectra of 5.0 M $NaPF_6$ solution. Peak area and width are plotted against the temperature for (A) OD_W, (B) OD_C, and (C) OD_A.

Figure 4. (A) Isotropic IR PP signal of 5.0 M $NaPF_6$ solution at 40 °C. IR PP signal is analyzed at two probe frequencies indicated by dashed lines. (B) Analysis of isotropic IR PP signal at the low frequency peak (OD_W + OD_C). (C) Analysis of isotropic IR PP signal at the high frequency peak (OD_A). The heating contribution, $G(t)$, was shown and subtracted for further analysis. See the text for detail.

Figure 5. Temperature-dependent IR PP experimental results for the low frequency peak at ~2530 cm^{-1} consisting of OD_W and OD_C. (A) Normalized vibrational population decays, $P(t)$, and (B) orientational anisotropy decays, $r(t)$, of aqueous 5.0 M $NaPF_6$ solution at different temperatures.

Figure 6. Temperature-dependent IR PP experimental results for the high frequency peak at ~2670 cm^{-1} (OD_A) (A) Normalized vibrational population decays, $P(t)$, and (B) orientational anisotropy decays, $r(t)$, of aqueous 5.0 M $NaPF_6$ solution at different temperatures.

Figure 7. Arrhenius plots for temperature-dependent orientational relaxation time for the low and high frequency peaks. From the slope, the activation energy for water orientation is obtained.

Figure 1.

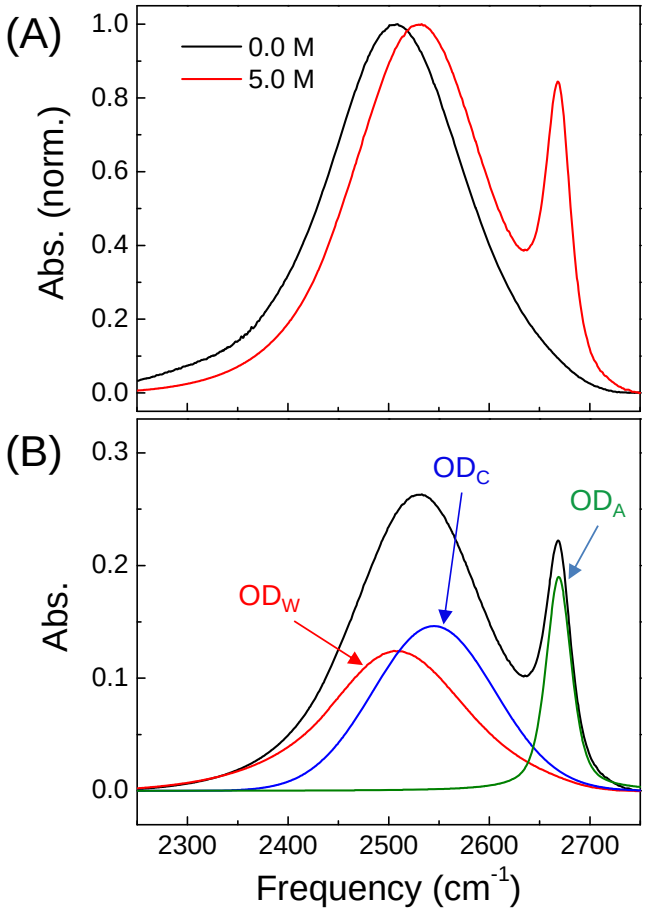

Figure 2.

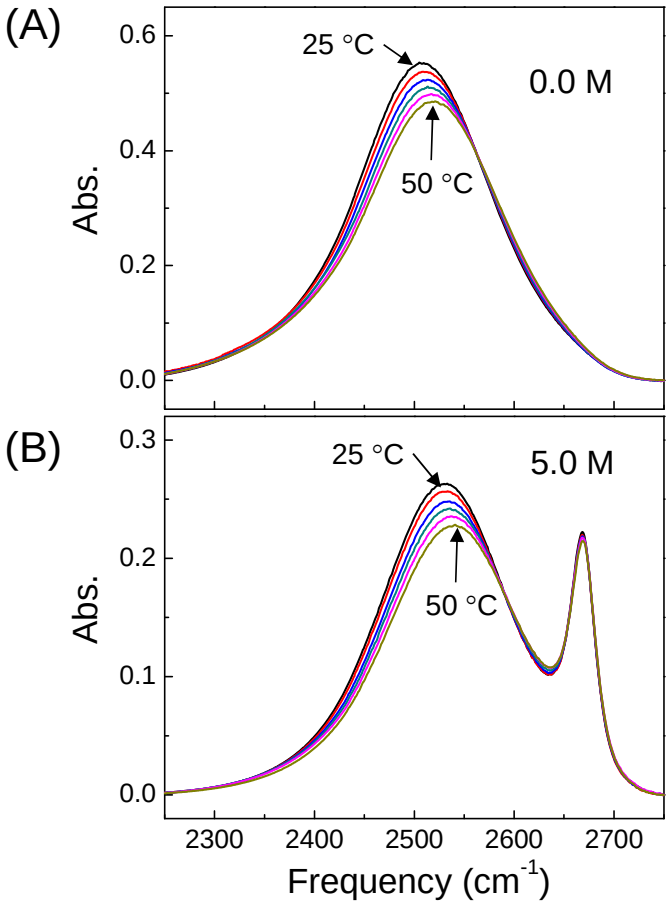

Figure 3.

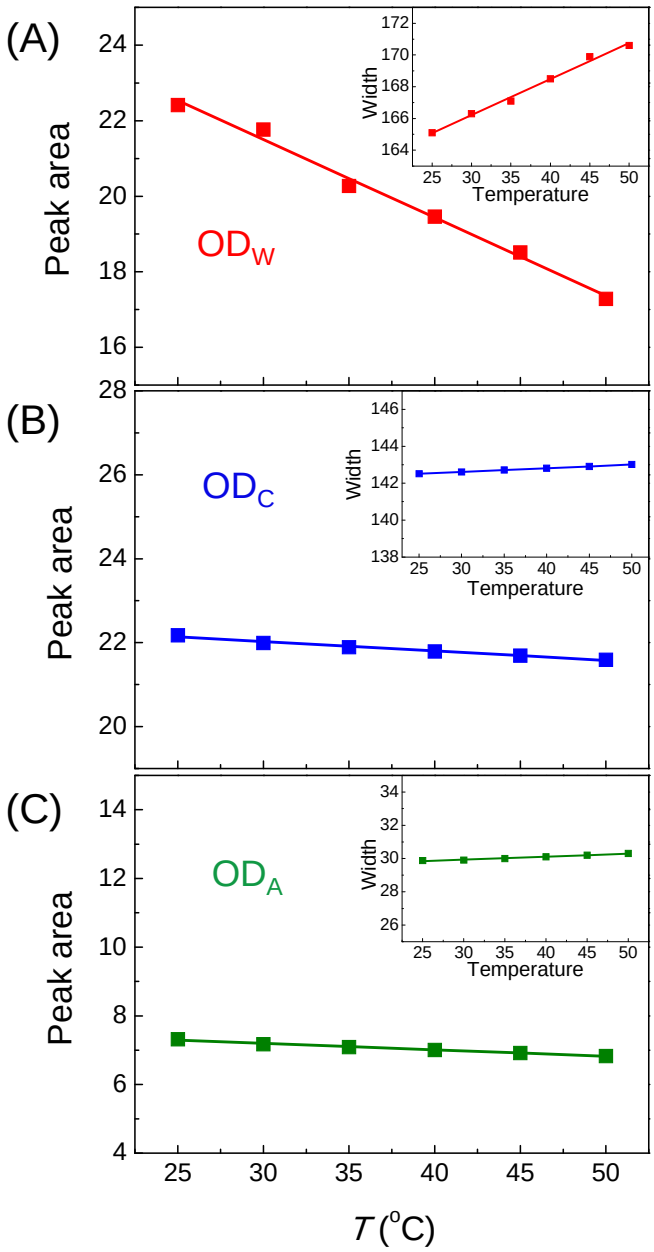

Figure 4

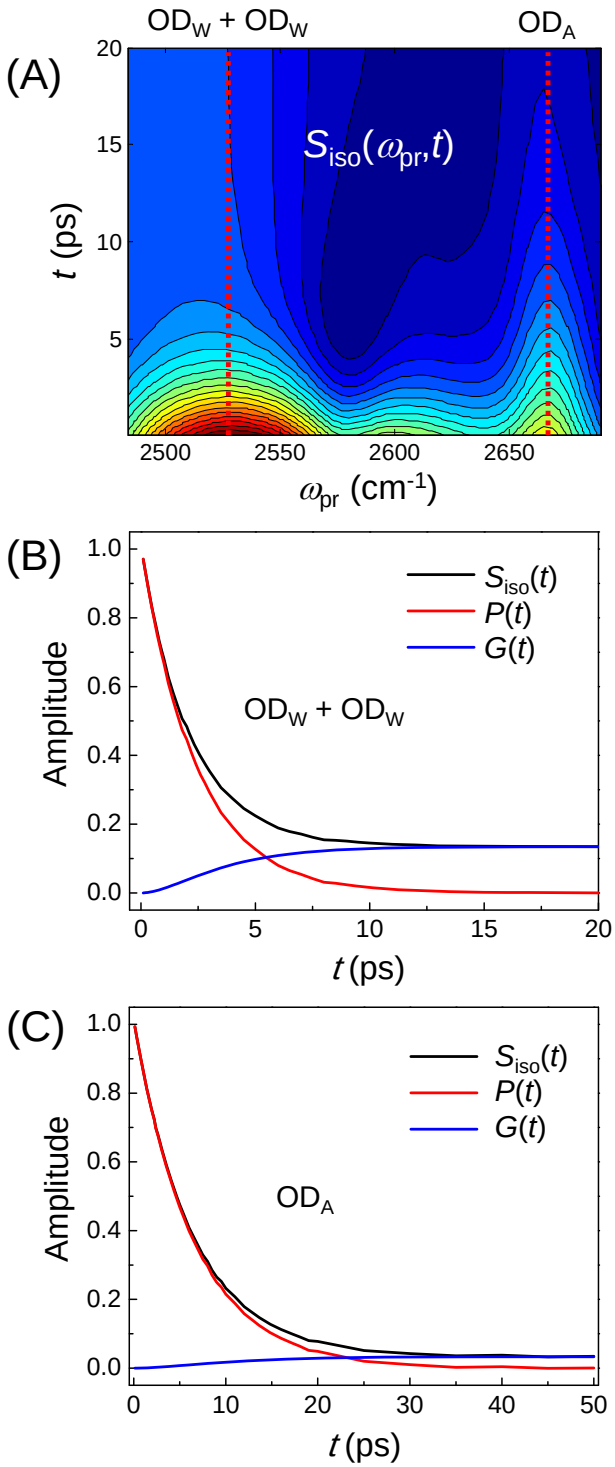

Figure 5.

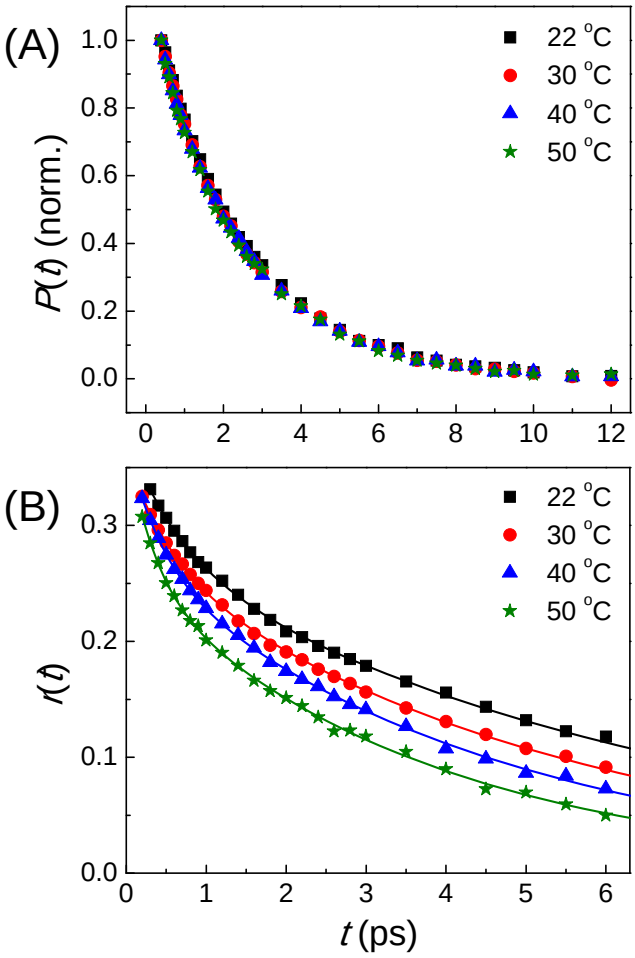

Figure 6.

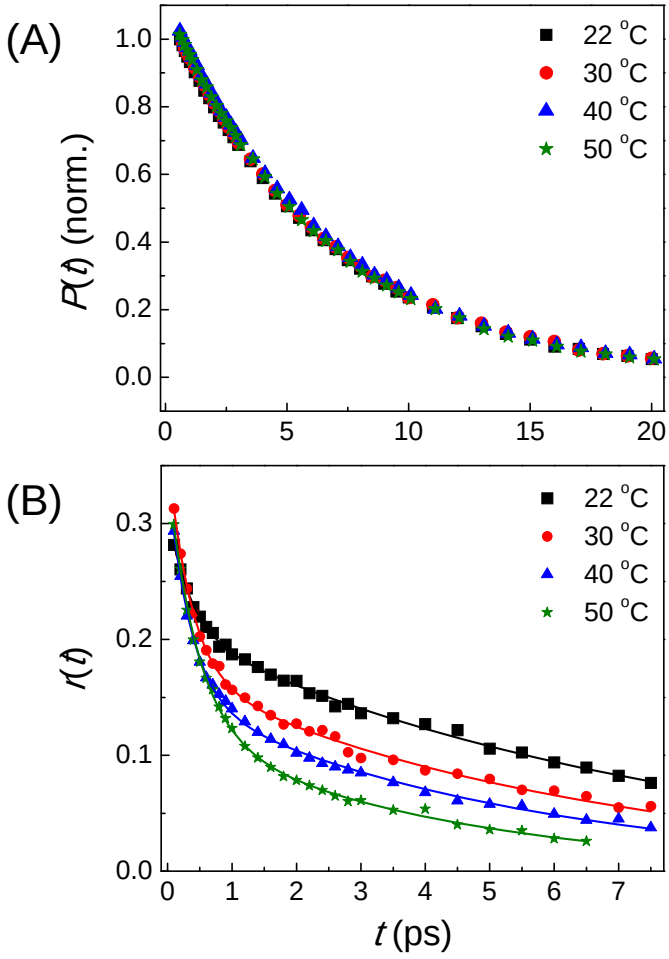

Figure 7.

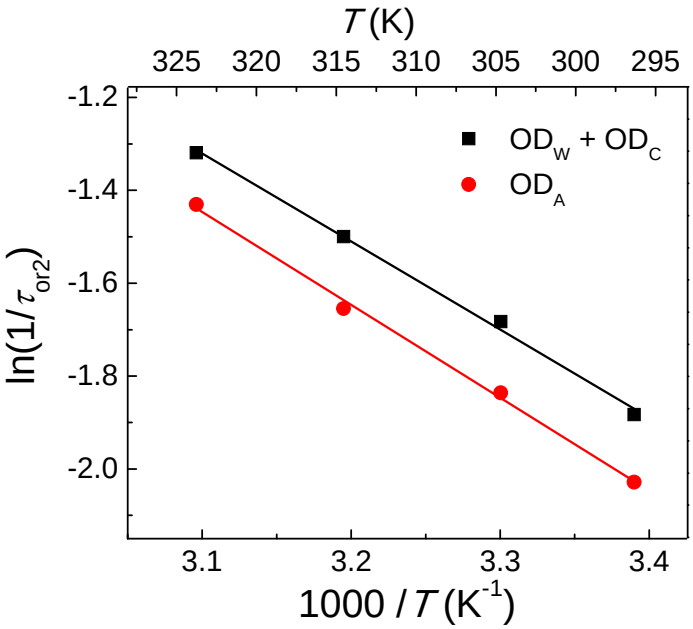

TOC graphic

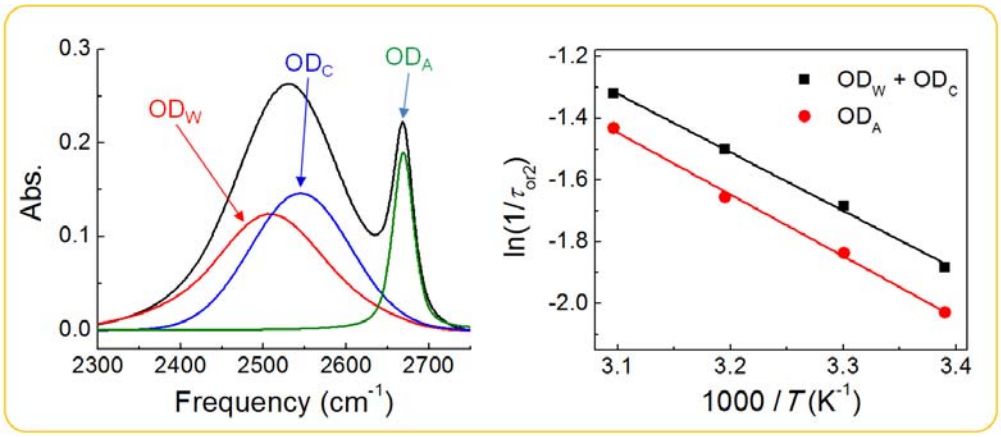

Structure and dynamics of water in aqueous PF_6^- solutions.